Nuclear Inst. and Methods in Physics Research, A 1017 (2021) 165806

Contents lists available at ScienceDirect

Nuclear Inst. and Methods in Physics Research, A

journal homepage: www.elsevier.com/locate/nima

Reconstruction of β-delayed neutron energy spectra from recoil-ion spectroscopy of trapped ions

G.L. Wilson [a,b,*], T.S. Nagel [c,d], S.T. Marley [a], N.D. Scielzo [d], A. Aprahamian [e], J.A. Clark [b], A. Czeszumska [d], G. Savard [b,f], K. Siegl [e,1], B.S. Wang [d]

[a] Department of Physics, Louisiana State University, Baton Rouge, LA 70803, USA
[b] Physics Division, Argonne National Laboratory, Lemont, IL 60439, USA
[c] Department of Nuclear Engineering, University of California, Berkeley, CA 94720, USA
[d] Lawrence Livermore National Laboratory, Livermore, CA 94550, USA
[e] Department of Physics, University of Notre Dame, Notre Dame, IN 46556, USA
[f] Department of Physics, University of Chicago, Chicago, IL 60637, USA

ARTICLE INFO

Keywords:
β-delayed neutron decay
Simulations
Recoil-ion spectroscopy
Paul trap

ABSTRACT

Beta-delayed one-neutron (βn) emission has been investigated by confining radioactive ions in an ion trap and detecting the β particles and recoiling nuclei that emerge following decay. In this approach, the βn energy spectrum and branching ratio can be deduced without needing to detect the neutrons, as the neutron emission is inferred from the observed time of flight of the recoiling ions. This paper details the dominant effects that influence the extraction of the neutron energy from the time-of-flight measurement and explores the impact they have on the energy calibration and resolution.

1. Introduction

Beta-delayed neutron (βn) emission is an energetically-viable process when the β-decay Q_β value of the parent (*precursor*) nucleus is greater than the neutron-separation energy (S_n) in the daughter (*emitter*) nucleus, populating states in the granddaughter (βn *daughter*) nucleus after neutron emission. This decay mode occurs in many neutron-rich nuclei that are more than a few nucleons off stability, and occurs with probability P_n, defined as the neutron-to-β emission branching ratio for the precursor. For β-delayed one neutron emission, the neutron-energy spectrum can extend up to $Q_{\beta\text{-}n} = Q_\beta - S_n - E_R$, where E_R is the small amount of energy imparted to the recoiling βn daughter nucleus. Decays which result in the emission of multiple neutrons will not be discussed in this paper as the recoil-ion spectroscopy method described here would need to be adapted for multiple neutron emission.

The βn process impacts applications of nuclear physics, such as nuclear-energy generation, and can yield valuable insights into the structure of nuclei and the production of heavy elements in the cosmos. For nuclear reactors, these delayed neutrons play a critically important role, as their contribution to the fission yield is essential for maintaining the stability of the fission chain reaction. Delayed neutrons limit the rate at which reactor power can drop, determined by the half-life of the longest lived precursor. They also contribute to the heat production in a reactor shortly after shutdown. Modern nuclear-reactor designs benefit from accurate nuclear data to ensure adequate safety margins, but there is limited information for P_n values and neutron-energy spectra for individual fission products. Nuclear data are also critical for improving nuclear structure and decay models, which in turn are used in simulations of the astrophysical rapid neutron capture (r) process [1,2]. The βn process impacts the latter stages of the r process during neutron *freeze out*, in which the flux of free neutrons rapidly decreases and nuclides β decay back to stability. The emission and capture of these neutrons can affect the mass flow back to stability and ultimately the final isobaric abundance pattern. Uncertainties in the βn properties used in global r-process models significantly affect calculated isobaric abundance patterns, and sensitivity studies have been undertaken to identify which individual βn precursors will have the most significant impact [3]. Currently, there are few measurements available [4], so studying the βn emission of these key precursors is vital to understand deficiencies in models that are used in r-process simulations.

Making precision measurements of βn emission is experimentally challenging. However, the use of atom and ion traps has opened up many new opportunities for precision β-decay studies [5]. These devices enable the determination of the low-energy nuclear recoil following decay, which allows for measurements of certain decay properties that would otherwise not be possible. For example, β-ν angular

* Corresponding author at: Department of Physics, Louisiana State University, Baton Rouge, LA 70803, USA.
E-mail address: gwilson@anl.gov (G.L. Wilson).
[1] Present address: Department of Physics and Astronomy, University of Tennessee, Knoxville, TN 37996, USA.

https://doi.org/10.1016/j.nima.2021.165806
Received 15 March 2021; Received in revised form 7 August 2021; Accepted 8 September 2021
Available online 14 September 2021
0168-9002/

correlations have been measured with magneto-optical traps [6–9] and Paul traps [10–12], and trapping has been employed to study the charge-state distribution of the daughter ions [13–17]; a review of the use of atom traps for studying β-decay angular correlations can be found in Refs. [5,18] and references therein.

Building on the successes of these precision measurements, a new recoil-ion spectroscopy approach to studying βn emission was demonstrated [19] by using the Beta-decay Paul Trap (BPT) [20]. This approach has recently been used to collect nuclear data on the βn emission of several isotopes [21,22] produced at the CAlifornium Rare Isotope Breeder Upgrade (CARIBU) at Argonne National Laboratory (ANL).

Recoil-ion spectroscopy avoids the difficulties inherent in direct neutron detection by instead inferring βn properties from the momentum imparted to the recoiling nucleus. By measuring the time of flight (TOF) of the recoiling ion following the detection of the β particle, βn events can be identified, and the neutron-energy spectrum can be reconstructed. As there are few backgrounds with similar TOF signatures, measurements can be made with beam intensities potentially as low as ~ 0.1 ions/s, which opens up a wide range of exotic nuclei for study.

The focus of this paper is on the phenomena that influence the reconstruction of the neutron energy from the measurement of the nuclear recoil. In a simple approximation, the momentum imparted to the recoiling βn daughter nucleus can be determined from the TOF and the distance traveled, and is equal and opposite to the momentum of the emitted neutron. However, considerations beyond this simple approximation give rise to shifts and broadening of the inferred neutron energy. These include experimental conditions, such as the spatial extent of the trapped-ion cloud and the RF field used to confine it, and the contributions from the emitted leptons, which depend on β-decay properties, such as Q_β and the angular correlations that arise between emitted particles. With existing data [14,21–23], these phenomena cannot be isolated and so simulations were employed to fully understand the magnitude of each contribution. The insights gained by doing so are imperative for designing future high-precision measurements of βn emission using this technique.

The effects of these phenomena on the inferred neutron energy, E_n', are quantified using simulations of ^{137}I, ^{99}Y, and ^{135}Sb βn decay in the BPT. These isotopes were selected to span a range of $Q_{\beta n}$ values (2002 ± 8, 2567 ± 11, and 4772 ± 4 keV, respectively [24]). In addition, the isotope ^{137}I has been well characterized with a variety of different techniques [25–27] and serves as an IAEA benchmark for βn emission in the heavy-mass peak of fission product distributions [28]; ^{99}Y is a precursor from the light-mass fission peak that is relevant for nuclear-energy studies [29–31]; and ^{135}Sb is the isotope with the largest $Q_{\beta n}$ value that has been measured in the BPT [22].

2. The recoil-ion spectroscopy method

The recoil ions emerging from the ion cloud following β and βn decay are distinguishable by their TOF; the emission of a neutron results in a higher recoil-ion momentum and energies typically extending up to tens of keV, compared to $\lesssim 500$ eV following β decay. In addition to the neutron-energy spectrum, P_n can also be extracted from the fraction of recoil ions with TOFs characteristic of βn emission. Suspending nuclei in a trap is critical for this method, as the use of any foil or target backing material would significantly perturb the recoil energies.

A Paul trap is employed to confine a cloud of singly-charged precursor ions in vacuum using time-varying electric fields. When a trapped ion decays, the emission of a β particle causes the ion charge state to increase by one unit (or more, if accompanied by the loss of atomic electrons) and the recoil energy imparted to the nucleus causes it to emerge from the trap confinement.

The neutron energy is related to the momenta of the decay products through the following relation:

$$E_n = \frac{|\vec{p}_R + \vec{p}_\beta + \vec{p}_{\bar{\nu}} + \sum \vec{p}_\gamma|^2}{2m_n} \tag{1}$$

where $\vec{p}_R$, $\vec{p}_\beta$ and $\vec{p}_{\bar{\nu}}$ denotes the momentum of the recoiling ion, β and $\bar{\nu}$, respectively, and $\sum \vec{p}_\gamma$ is the summed momenta of all emitted γ rays. Due to the relative sizes of the neutron and lepton momenta, the decay kinematics of the neutron and recoiling βn daughter nucleus is nearly back-to-back; in the approximation that the lepton and γ-ray contribution to the nuclear recoil can be neglected, the neutron momentum $\vec{p}_n$ is equal and opposite to $\vec{p}_R$ and

$$E_n \approx \frac{|\vec{p}_R|^2}{2m_n}. \tag{2}$$

As a concrete example, the most intense βn feature in the decay of ^{137}I is the emission of a 377-keV neutron from a 4400-keV state in ^{137}Xe, to the ^{136}Xe ground state. In the case where the β particle is emitted with the maximum kinetic energy (e.g. $E_\nu = 0$), then $E_\beta = 1622$ keV from the energy difference between $Q_{\beta n}$, E_n and the energy of the recoiling βn daughter nucleus, E_R. In this case, $p_\beta = 2.1\,\mathrm{MeV}/c$ is more than an order of magnitude smaller than the momentum, $p_n = 26.6\,\mathrm{MeV}/c$, for the 377-keV neutron. The energy sharing between the particles and the relative orientation of their momenta in Eq. (1) affects the recoil energy (and hence the reconstruction of E_n) and will be discussed in Section 4.

2.1. The Beta-decay Paul Trap

The BPT [20] was originally designed and built to measure β-decay angular correlations [10,12] for tests of the Standard Model, and also has been adapted for βn studies. The BPT is a linear radio-frequency quadrupole (RFQ) trap that is used to confine a $\sim 1\,\mathrm{mm}^3$ cloud of precursor ions. The trapping potential for the BPT, determined from the Mathieu equations [32], was chosen such that low-energy precursor ions in a 1^+ charge state delivered to the trap would be stably confined, but recoiling ions following β decay, which have charge states 2^+ and higher, would not, regardless of their energy. The planar trap electrodes have an open design allowing detectors to be placed in a box geometry around the ion cloud, shown in Fig. 1. Two ΔE-E plastic scintillator telescopes placed at 90° to each other ('top' and 'left' with respect to the beam) allow for the detection of the β particle, with the ΔE detector providing the start signal for the TOF measurement. The other two sides of the box geometry ('bottom' and 'right') have resistive-anode position-sensitive microchannel plate (MCP) detectors to detect the low-energy ions emitted following decay. The momentum of the recoil-ion $\vec{p}_R$ can be determined from the distance d and time of flight t of the recoiling ion's trajectory from the ion cloud to the impact location on the MCP detector, and therefore the inferred neutron energy $E_n' = M_R^2(d/t)^2/2m_n$. The detectors are oriented such that the β-ion coincidences can be detected over a range of angles centered at 90° and 180°.

2.2. Simulations of β and βn decay in the BPT

Simulations of the recoil-ion trajectories in the electric field and the particle energy depositions in detectors were undertaken using the SimIon 8.1 [33] and GEANT4 [34] simulation packages, respectively. The β-decay input was produced with an event generator, originally developed for β-ν angular correlations [13,35] and adapted for βn emission [19]. For each precursor, decays are generated using an allowed β-decay energy spectrum to a set of excited states in the emitter nucleus as defined by the user. Allowed Gamow-Teller (GT) decays of 1^+ precursor ions to emitters with a charge state of 2^+ were simulated in each case. The phase space, $W(\theta)$, for βn decay is given by

$$W(\theta) \propto 1 + a_{\beta\nu}\frac{\vec{p}_\beta}{E_\beta}\cos(\theta_{\beta\bar{\nu}}) + G_{12}\frac{\vec{p}_\beta}{E_\beta}\left[\cos(\theta_{\beta n})\cos(\theta_{n\bar{\nu}}) - \frac{1}{3}\cos(\theta_{\beta\bar{\nu}})\right], \tag{3}$$

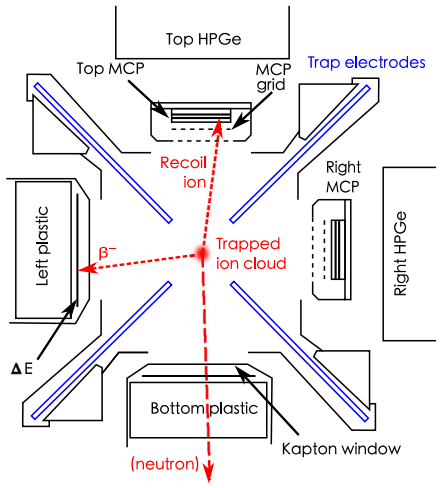

Fig. 1. A cross-sectional view of the BPT setup (not to scale), depicting an example of a β-delayed neutron event with dashed arrows.
Source: Figure adapted from Ref. [21].

which is adapted from Ref. [36] and neglects the recoil-order terms[2]. For these GT decays, the β-ν correlation coefficient $a_{\beta\nu} = -\frac{1}{3}$ and the spins accessible are restricted. The β-$\bar{\nu}$-n triple correlation, with θ_{xy} as the angle between emitted particles x and y, arises because the leptons carry away angular momentum and leave the spin of daughter nucleus oriented. As a result, this correlation depends on the spin sequence of the βn decay, where j' and j'' represent the spins of the emitter and βn-daughter nuclei, respectively, and on the neutron orbital angular momentum, L. The coefficient for this term is typically of order unity and is determined by $G_{12} \equiv \frac{1}{10} g_{12} \tau_{j'j''}$, where the factors g_{12} and $\tau_{j'j''}$ are defined in Refs. [12,36]. Previous work has shown [14,15,37–39] that β decay leads to a charge-state distribution of the recoiling ions resulting from the loss of atomic electrons, but the most likely outcome is that all the atomic electrons are retained. For simplicity, here the 2^+ charge state, in which all the atomic electrons are retained, was the focus of this work. Simulations indicate that the energy imparted to a recoiling ion following βn decay is great enough that its charge does not significantly affect the trajectory.

The BPT detector setup and trap voltages are based on the configuration used at CARIBU [14,21–23] in order for the simulations to represent realistic experimental conditions. The central $46 \times 46\,\text{mm}^2$ of the MCP detector was used as the fiducial area in the data analysis [14], and each MCP was placed 52.0(3) mm away from trap center. A pulse-height threshold was applied to the MCP signals and a β-energy threshold of 75 keV was applied to the plastic-scintillator ΔE-detector signals [21,40]. To explore the neutron-energy reconstruction, β decays populating individual, highly-excited states were simulated, occurring in an ion cloud with a Gaussian distribution at the trap center with a full width at half maximum (FWHM) of $\sim$ 1 mm in all three spatial dimensions. The simulated states were chosen so that neutrons were emitted with energies at regularly-spaced energy intervals up to $\sim$ 500 keV lower than the $Q_{\beta n}$ value for each precursor (above that energy, the efficiency for detecting β-ion coincidences drops rapidly because of the β-particle detection threshold). Details of the events simulated are discussed with the individual results.

3. Determination of the recoil-ion momentum

The recoil-ion momentum is determined from the TOF and the distance traveled by the recoiling ion, and the uncertainty in these quantities determines the resolution with which the momentum can be reconstructed.

The TOF resolution is determined by the 3-ns FWHM timing resolution achieved with the coincident detection system consisting of ΔE plastic scintillators (TOF start) and MCP detectors (TOF stop). This resolution yields a 1% timing spread for the shortest TOFs of 300 ns, and an even smaller fractional spread for the longer TOFs. A 3-ns FWHM Gaussian timing resolution has been applied to the TOF used to reconstruct the neutron-energy spectra in Fig. 2. The effect of the timing resolution is minimal except at the highest neutron energies, but even there it is considerably smaller than the effect from the ion cloud size, which will be discussed later in this section.

The −2.5-kV MCP bias voltage accelerates the ions and increases their energy for detection. A grounded 89% transmission grid, mounted 4.5 mm in front of the MCP, prevents the recoil ions from being perturbed by the MCP bias for most of their trajectory. The impact the MCP bias voltage has on decreasing the TOF after the ions pass through the grid is calculated analytically, as the force on the ion from the approximately uniform electric field in that region is known (details of which can be found in Ref. [41], Appendix D). For the full range of TOFs observed in the experiment, the TOF correction for recoil ions is on the order of $\sim$0.6–4.6%, which corresponds to an energy correction of 1.2–9.3% [40].

The distance depends on the ion cloud size as well as the trajectory, which we approximate as a straight line from the trap center to the impact position on the MCP detector. Although the RF fields perturb the trajectories, simulations indicated that this effect has a negligible impact on the reconstructed ion momentum; simulations without RF reproduce the TOF peak for the recoil ions, and so the straight line trajectory assumption is valid. The MCP detectors have a position resolution significantly better than 1 mm (position calibration details given in Ref. [41]), which at a distance of 53 mm from trap center, yields a relative uncertainty in the distance measurement of $< 1\%$ in the most extreme case of a recoil ion hitting one corner of the MCP fiducial area.

The impact an ion-cloud size of $\sim$ 1 mm FWHM in all three dimensions [14] has on the E_n' spectrum was investigated with simulations. Fig. 2 shows the results of a simulation of monoenergetic neutrons emitted following the βn decay of the precursor ^{137}I, resulting in ^{136}Xe ions of charge state 2^+. Neutrons were generated with energies at 200-keV intervals, up to 1800 keV. The spectra are generated under identical conditions except for the initial decay locations which was set to be either a point source (Fig. 2*a–d*) or an extended ion cloud described by a 1-mm FWHM Gaussian distribution in all three spatial directions (Figs. 2*e*, 2*f*).

The location of the decay position within the ion cloud is the dominating uncertainty in determining the distance traveled by the recoiling ion. For a 1-mm^3 ion cloud, the broadening increases linearly with E_n, dominating the resolution at high neutron energies. Fig. 2 also shows how well the average value for the reconstructed E_n' matches the true E_n; these agree well for the 90° detector combination, but for the 180° detector combination, a minor shift in E_n' is due to the additional momentum imparted by the leptons. A point-like ion cloud will be used for the subsequent investigations to better isolate the impact of the other contributions.

4. Lepton recoil

The emission of the β and $\bar{\nu}$ contribute to the total momentum imparted to the recoil ion, which in turn affects the E_n' reconstruction, as shown in Eq. (1). For $E_n \gtrsim 100$ keV, the neutron momentum is much larger than that of the leptons or γ rays, and so $\vec{p}_R$ is dominated by the neutron. However, if the recoil energy is solely ascribed to the neutron, this typically causes an overestimation of E_n'.

The orientation of $\vec{p}_\beta$ and $\vec{p}_{\bar{\nu}}$ influences the size of this effect. The triple correlation is complicated, but a positive G_{12} value leads to an

[2] Equation (53) of Ref. [36] requires a correction in the sequential numbering of spectral functions: the second instance of g_{11} should be g_{12}, g_{12} should be g_{13}, and g_{13} should be g_{14}.

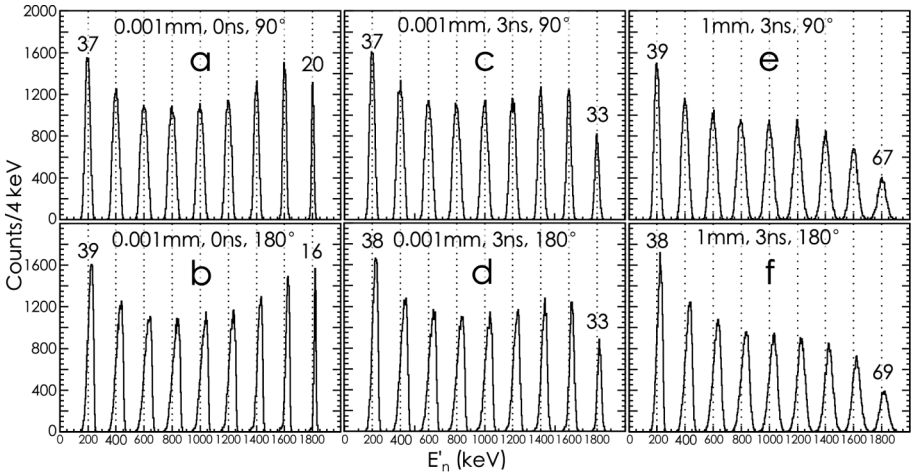

Fig. 2. Simulations of reconstructed monoenergetic neutron-energy (E'_n) spectra for 2^+ recoil ions following the βn decay of ^{137}I. Vertical dotted lines represent the true energy (E_n) of the emitted neutron. The results in (a) to (d) are for a point-like ion cloud, where panels (c) to (f) also incorporate a 3-ns timing resolution (see text), and (e) and (f) are for a cloud with 1 mm FWHM in all three dimensions. The results in (a), (c) and (e) are for the detector combinations at 90° and in (b), (d) and (f) are for the detector combinations at 180°. The numbers above the 200- and 1800-keV peaks are the FWHM for those peaks in keV. Energy thresholds have been applied; see text.

Table 1
Calculated G_{12} values for different precursor to emitter to βn daughter ($j \to j' \to j''$) spin sequences. The lowest values of the neutron orbital angular momentum L are listed. The angular momentum of the final nucleus coupled to the neutron spin can have multiple values for the same L, leading to multiple values of G_{12}.

	$j \to j' \to j''$	L	$G_{12} \equiv \frac{1}{10} g_{12} \tau_{j' j''}$
^{137}I	$\frac{7}{2}^+ \to \frac{5}{2}^+ \to 0^+$	2	0.2857
	$\frac{7}{2}^+ \to \frac{7}{2}^+ \to 0^+$	4	−0.9524
	$\frac{7}{2}^+ \to \frac{9}{2}^+ \to 0^+$	4	0.667
^{99}Y	$\frac{5}{2}^+ \to \frac{3}{2}^+ \to 0^+$	2	0.2
	$\frac{5}{2}^+ \to \frac{5}{2}^+ \to 0^+$	2	−0.9143
	$\frac{5}{2}^+ \to \frac{7}{2}^+ \to 0^+$	4	0.4188
^{135}Sb	$\frac{7}{2}^+ \to \frac{5}{2}^+ \to 0^+$	2	0.2857
	$\frac{7}{2}^+ \to \frac{7}{2}^+ \to 0^+$	4	−0.9524
	$\frac{7}{2}^+ \to \frac{9}{2}^+ \to 0^+$	4	0.667
	$\frac{7}{2}^+ \to \frac{5}{2}^+ \to 2^+$	0	0
	$\frac{7}{2}^+ \to \frac{7}{2}^+ \to 2^+$	2	−0.1361 ($5/2^+$) −0.8163 ($3/2^+$)
	$\frac{7}{2}^+ \to \frac{9}{2}^+ \to 2^+$	2	0.5238
	$\frac{7}{2}^+ \to \frac{5}{2}^+ \to 4^+$	2	0.102 ($9/2^+$) −0.1735 ($7/2^+$)
	$\frac{7}{2}^+ \to \frac{7}{2}^+ \to 4^+$	0	0
	$\frac{7}{2}^+ \to \frac{9}{2}^+ \to 4^+$	0	0

average increase in the recoil kick from the leptons, and causes an overestimation of E_n. Thus a larger lepton recoil correction is needed. This increase in recoil energy can be as high as 36% for the limiting case of a 100-keV neutron from the βn emission of ^{135}Sb, as shown in Fig. 3, but only a 1% increase for a 4-MeV neutron using identical simulation parameters. The effect is much smaller when $G_{12} < 0$; the recoil ion will receive a smaller kick from the leptons, and E'_n will be close to E_n. As multiple decay paths and spin sequences are possible from the precursor to the emitter to the βn daughter, and the relative contributions of each decay path are unknown, we use an average value of the accessible G_{12} values for the decay. This results in an uncertainty on the lepton–recoil correction and a contribution to the experimental E_n resolution. The simulations show the accuracy of E'_n, but also any effects on the resolution. In Fig. 2(*b*) and (*d*), the data from the 180° detector pairs have a pronounced shift in the reconstructed E_n from the true value, due to the lepton recoil not being taken into account.

Table 1 shows the possible spin sequences, from precursor to emitter to βn-daughter, for the precursors investigated in this work. For the case of ^{137}I we assume that 100% of the ^{137}Xe neutron-emission strength goes to the 0^+ ground state in ^{136}Xe. Experimental results [42] show that very little of the decay strength goes to the first-excited state, which is the only other accessible state. As the ^{137}I ground state J^π is $7/2^+$, allowed GT decay selection rules permit the daughter to populate states with spins $9/2^+$, $7/2^+$, or $5/2^+$. For the parity to remain unchanged in the transition to the 0^+ state in ^{136}Xe, the emitted neutron must have even values of angular momentum $L \geq 2$ if emitted from the $5/2^+$ state, and even values of $L \geq 4$ if emitted from the $7/2^+$ or $9/2^+$ states. We assume that the nucleus will preferentially emit neutrons with the smallest allowable orbital angular momentum L in each case. The corresponding values for G_{12} for each possible spin sequence have been calculated using the equations in Ref. [36] for the lowest L, and the results are shown in Table 1.

In the case of ^{137}I, and similarly for ^{99}Y, this process is relatively straightforward, as only one state is assumed to be populated in the βn daughter, and only one L value is possible. The case is more complicated for ^{135}Sb, as there are a number of low-lying excited states in the βn daughter ^{134}Te that are energetically accessible, and experiments indicate that the first and second excited states are populated along with the ground state [43]. There are also two cases in which the angular momentum of the final nucleus coupled to the neutron spin can have multiple values for the same L, which leads to multiple values of G_{12}. The effect of the β-$\bar{\nu}$-n correlation is investigated by simulating the βn decay using the minimum and maximum value of G_{12} in Table 1 for each precursor.

4.1. E_n shifts due to lepton recoil

Fig. 3 shows the ratio E'_n to E_n as a function of E_n for the precursors ^{137}I, ^{99}Y, and ^{135}Sb. The value deviates from unity due primarily to the lepton contribution to the total recoil-ion momentum; the magnitude of this E_n-dependent deviation from unity is then used to correct the experimental E_n spectrum. This effect is largest for β-ion coincidences detected in the 180° detector pair where the neutron and β-particle momenta are somewhat aligned, leading to the recoil from both particles adding constructively. This leads to E'_n as determined from Eq. (1) overestimating E_n because it ascribes all the recoil energy to the neutron. This effect is most pronounced at the lowest neutron energies where the neutron momentum is smallest and the average β-particle energy is largest. As E_n increases, $p_n \gg p_\beta$ and the ratio approaches unity. The average momentum imparted by the leptons to the recoil ion is dependent on the energy available to the leptons ($Q_{\beta n} - E_n$). As shown in Fig. 3, the energy shifts for the three precursors display the same E_n and G_{12} dependencies but are scaled overall by a factor approximately proportional to $Q_{\beta n} - E_n$.

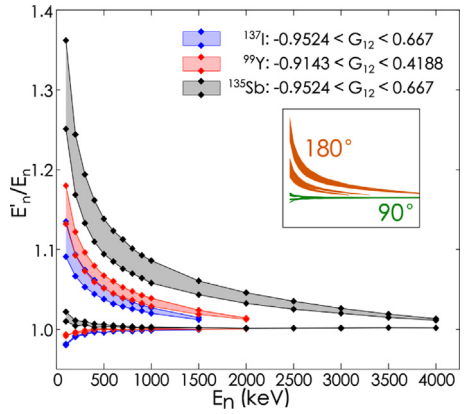

Fig. 3. Simulated results for E_n'/E_n as a function of E_n for ^{137}I (blue), ^{99}Y (red), and ^{135}Sb (black), separated into 90° and 180° detector pairs. For clarity, the two extreme G_{12} values form the lower and upper boundaries of a colored region corresponding to the full range of energy shifts possible due to the lepton recoil. (For interpretation of the references to color in this figure legend, the reader is referred to the web version of this article.)

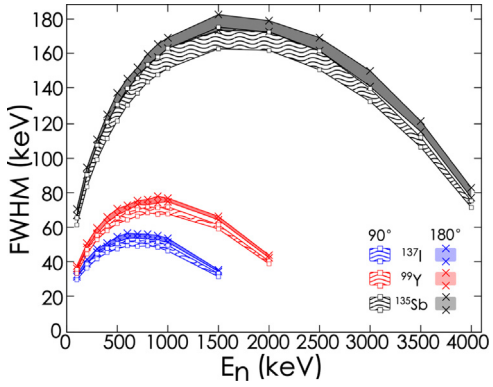

Fig. 4. Neutron energy resolutions for ^{137}I (blue), ^{99}Y (red), and ^{135}Sb (black), obtained from simulations. Results for the 90° and 180° detector pairs plotted separately. The bounds of the shaded regions correspond to the upper and lower possible G_{12} values, see text. (For interpretation of the references to color in this figure legend, the reader is referred to the web version of this article.)

4.2. Energy resolution

The effect of the β-$\bar{\nu}$-n correlation on the resolution of the reconstructed neutron energy was investigated via simulation. Fig. 4 shows the range of FWHM values of each E_n' peak, given the range of G_{12} values possible for each decay sequence. Data corresponding to detector pairs at 90° and 180° are again plotted separately with the boundaries of the shaded regions indicating the upper and lower G_{12} values. The reconstructed neutron energy is corrected using the shift for the average G_{12} coefficient, and therefore the resolution of the reconstructed neutron energy is limited by this small spread. A more realistic idea of the resolution of the reconstructed neutron energy peaks can be achieved by folding in the effect of the ion cloud, as this physical effect cannot be corrected in analysis. Fig. 5 shows the difference in the energy resolution between a point-like ion cloud and a 1-mm^3 FWHM ion cloud. In each case, the larger ion-cloud size contributes significantly to the inferred neutron-energy resolution at the neutron energies at the higher-energy half of the spectrum.

5. Neutron–ion coincidences

A source of background arises from events where the neutron triggers a ΔE detector. Due to the neutron and recoiling ion being nearly back-to-back, when a recoiling ion is detected in an MCP detector, the opposite ΔE detector will almost certainly be hit by the neutron, and the event may be misidentified as a β-ion coincidence. The thin ΔE detector (10.6 cm in diameter, 1 mm thick) was designed to trigger on β particles while having a small intrinsic efficiency for detecting γ rays and neutrons. In addition, the proton recoils from neutron interactions in the scintillator generate significantly less light than electron interactions [44]. As a result, a 75 keV β-particle threshold corresponds to effectively 350 keV for neutrons and simulations indicate the intrinsic efficiency for detecting a 1 MeV neutron is ~ 1.5%. However, the back-to-back correlation of the neutron–ion events enhances their detection rate in the 180° detector pairs, and this background needs to be understood.

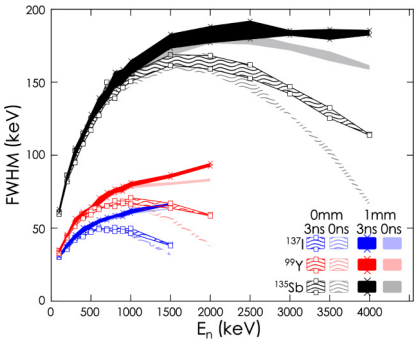

Fig. 5. A summary of the reconstructed neutron-energy resolution as a function of E_n obtained from the simulations of ^{137}I (blue), ^{99}Y (red) and ^{135}Sb (black). Solid loci represent the neutron-energy resolution when all phenomena have been taken into account, including a 1-mm^3 ion cloud size and a 3-ns timing resolution. These are compared to a 1-mm^3 ion cloud with no timing resolution (light shading), and a 0-mm^3 ion cloud with and without timing resolution (patterned and light patterned, respectively). For clarity, only data from 90° detector pairs are plotted; the 180° detector results are nearly identical. The two extreme G_{12} values for each precursor form the upper and lower boundaries of the shaded regions, see text. (For interpretation of the references to color in this figure legend, the reader is referred to the web version of this article.)

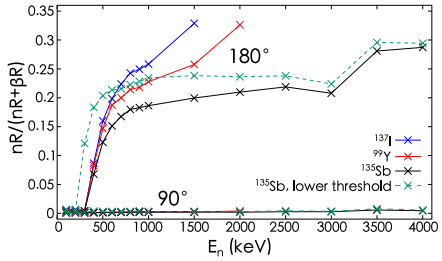

Fig. 6. Ratio of neutron–recoil ion coincidences (nR) to the total particle–recoil ion coincidences ($nR+\beta R$) as a function of simulated E_n, using the same simulated data as in Figs. 3 and 4, with $G_{12} = 0$ and a point-like ion cloud. Results with solid lines have a neutron-energy and β-energy threshold of 350 and 75 keV, respectively, whereas the dashed line uses the lower thresholds of 230 and 50 keV for ^{135}Sb (see text).

This type of event has been investigated through simulations, in which it is possible to distinguish between a neutron and a β in the ΔE detector. Fig. 6 shows the expected proportion of coincidence events that are neutron–recoil ion (nR) pairs rather than β–recoil ion (βR) pairs, as a function of the simulated neutron energy. The effects of the 350-keV neutron-energy threshold is clear in reducing the number of nR coincidences.

For a future detector system, a lower β-energy threshold would be preferable. However, this would also lead to a lower neutron-energy threshold, which would increase the number of neutron–ion coincidences, and so some discrimination between neutrons and β particles would be needed to minimize this background. For a 50-keV β-energy threshold, the neutron-energy threshold would be expected to be about

230 keV [40,44], based on scaling the energies. The $nR/(nR + \beta R)$ proportion as a function of E_n for these lower thresholds is shown in Fig. 6. The corresponding simulations of ^{137}I and ^{99}Y with lower thresholds show the same trends. The resulting neutron energy spectra inferred from the 180° detector pairs need to take into account the added efficiency for detecting these events.

6. Conclusions and outlook

An ion trap has been successfully employed to measure β-delayed single-neutron emission using recoil-ion spectroscopy, allowing both the neutron-energy spectrum and the probability of β-delayed neutron emission to be inferred without directly detecting the neutron. In this work, we have explored the physics and experimental corrections needed to infer the neutron energy from the time-of-flight of the recoiling ions emerging from the trapped-ion cloud. We have performed simulations of three βn precursors (^{137}I, ^{99}Y, and ^{135}Sb) to investigate the energy calibration and the resolution of the inferred neutron-energy spectrum. This work provides insight into how to improve the quality of the neutron spectra obtained with this approach.

The size of the ion cloud was shown to have a significant effect on the neutron energy resolution, particularly for neutron energies approaching the $Q_{\beta-n}$ value, where the FWHM almost doubles. The reconstructed neutron energy can be improved by minimizing the size of the ion cloud with a cryogenically-cooled He buffer gas [12].

The momentum imparted by the leptons on the recoiling ion was shown to cause an overestimation of the reconstructed neutron energy by as much as 36% for β–recoiling ion coincidences detected in a MCP-ΔE detector pair 180° apart; whilst coincidences seen in the 90° detector pair are essentially unaffected by this effect. Knowledge of this overestimation allows for accurate correction to experimental neutron spectra; although this shift can be corrected, there is uncertainty in its exact size due to different angular correlations that arise between the emitted particles. Triple (β-$\bar{\nu}$-n) correlations were also shown to contribute to the lepton recoil effect by as much as a few percent.

The background caused by neutrons incident on the ΔE detectors can be characterized by segmenting the ΔE detectors. Based on the likelihood of detecting neutron–recoil-ion pairs 180° apart, spatial information on the ΔE detector on the order of a few centimeters would be sufficient to discriminate between β–recoil-ion pairs and neutron–recoil-ion pairs, which can be achieved with segmentation.

CRediT authorship contribution statement

G.L. Wilson: Software, Validation, Formal analysis, Investigation, Data curation, Writing – original draft, Writing – review & editing, Visualization, Project administration, Conceptualization. **T.S. Nagel:** Software, Investigation, Writing – original draft. **S.T. Marley:** Supervision, Funding acquisition, Writing – original draft, Conceptualization. **N.D. Scielzo:** Conceptualization, Methodology, Writing – original draft, Writing – review & editing, Supervision, Project administration, Funding acquisition. **A. Aprahamian:** Funding acquisition. **J.A. Clark:** Resources. **A. Czeszumska:** Software, Validation. **G. Savard:** Resources, Writing – review & editing. **K. Siegl:** Software, Validation, Writing – review & editing. **B.S. Wang:** Software, Validation, Writing – review & editing.

Declaration of competing interest

The authors declare that they have no known competing financial interests or personal relationships that could have appeared to influence the work reported in this paper.

Acknowledgments

We thank Grigor Sargsyan and Kristina Launey for productive discussions about β-$\bar{\nu}$-n triple correlations. This work was supported by the Louisiana State Board of Regents Research Competitiveness Subprogram, United States under award LEQSF(2016-19)-RD-A-09; the National Nuclear Security Administration, United States under Grant No. DE-NA0000979 (National Nuclear Security Consortium), and Contract Nos. DE-AC52-07NA27344 (Lawrence Livermore National Laboratory, United States); the United States Department of Energy, Office of Science, Office of Nuclear Physics under Contract No. DE-AC02-06CH11357 (Argonne National Laboratory); NSF, United States contract PHY-1419765, and by the National Science Foundation, United States under Grant PHY-1713857 (University of Notre Dame) and JINA-CEE NSF Physics Frontier Center, United States PHY-1430152 (University of Notre Dame).

References

[1] M.R. Mumpower, R. Surman, G.C. McLaughlin, A. Aprahamian, The impact of individual nuclear properties on r-process nucleosynthesis, Progr. Part. Nucl. Phys 86 (2016) 86–126.

[2] T. Marketin, L. Huther, G. Martínez-Pinedo, Large-scale evaluation of β-decay rates of r-process nuclei with the inclusion of first-forbidden transitions, Phys. Rev. C 93 (2016) 025805.

[3] R. Surman, M.P. Mumpower, A. Aprahamian, The sensitivity of r-process nucleosynthesis to individual β-delayed neutron emission probabilities, JPS Conf. Proc. 6 (2015) 010010.

[4] P. Dimitriou, I. Dillman, B. Singh, V. Piksaikin, K.P. Rykaczewski, J.L. Tain, et al., Development of a reference database for beta-delayed neutron emission, Nucl. Data Sheets 173 (2021) 144–238.

[5] J.A. Behr, A. Gorelov, D. Melconian, M. Trinczek, W.P. Alford, D. Ashery, P.G. Bricault, L. Courneyea, J.M. D'Auria, J. Deutsch, J. Dilling, M. Dombsky, P. Dubé, F. Glück, S. Gryb, S. Gu, O. Haüusser, K.P. Jackson, B. Lee, A. Mills, E. Paradis, M.R. Pearson, R. Pitcairn, E. Prime, D. Roberge, T.B. Swanson, Weak interaction symmetries with atom traps, Eur. Phys. J. A. 25 (2005) 685–689.

[6] P.A. Vetter, J.R. Abo-Shaeer, S.J. Freedman, R. Maruyama, Measurement of the β-ν correlation of ^{21}Na using shakeoff electrons, Phys. Rev. C 77 (2008) 035502.

[7] J.A. Behr, A. Gorelov, K.P. Jackson, M.R. Pearson, M. Anholm, T. Kong, R.S. Behling, B. Fenker, D. Melconian, D. Ashery, G. Gwinner, TRINAT: measuring β-decay correlations with laser-trapped atoms, Hyperfine Interact. 225 (2014) 115–120.

[8] A. Gorelov, D. Melconian, W.P. Alford, D. Ashery, G. Ball, J.A. Behr, P.G. Bricault, J.M. D'Auria, J. Deutsch, J. Dilling, M. Dombsky, P. Dubé, J. Fingler, U. Giesen, F. Glück, S. Gu, O. Haüusser, K.P. Jackson, B.K. Jennings, M.R. Pearson, T.J. Stocki, T.B. Swanson, M. Trinczek, Scalar interaction limits from the β-ν correlation of trapped radioactive atoms, Phys. Rev. Lett. 94 (2005) 142501.

[9] B. Fenker, J.A. Behr, D. Melconian, R.M.A. Anderson, M. Anholm, D. Ashery, R.S. Behling, I. Cohen, I. Craiciu, J.M. Donohue, C. Farfan, D. Friesen, A. Gorelov, J. McNeil, M. Mehlman, H. Norton, K. Olchanski, S. Smale, O. Thériault, A.N. Vantyghem, C.L. Warner, Precision measurement of the nuclear polarization in laser-cooled, optically pumped ^{37}K, New J. Phys. 18 (2016) 073028.

[10] G. Li, R. Segel, N.D. Scielzo, P.F. Bertone, F. Buchinger, S. Caldwell, A. Chaudhuri, J.A. Clark, J.E. Crawford, C.M. Deibel, J. Fallis, S. Gulick, G. Gwinner, D. Lascar, A.F. Levand, M. Pedretti, G. Savard, K.S. Sharma, M.G. Sternberg, T. Sun, J.V. Schelt, R.M. Yee, B.J. Zabransky, Tensor interaction limit derived from the α-β-ν correlation in trapped ^{8}Li ions, Phys. Rev. Lett. 110 (2013) 092502.

[11] X. Fléchard, P. Velten, E. Liénard, A. Méry, D. Rodríguez, G. Ban, D. Durand, F. Mauger, O. Naviliat-Cuncic, J.C. Thomas, Measurement of the β-ν correlation coefficient $a_{\beta\nu}$ in the β decay of trapped ^{6}He^{+} ions, J. Phys. G: Nucl. Part. Phys 38 (2011) 055101.

[12] M.G. Sternberg, R. Segel, N.D. Scielzo, G. Savard, J.A. Clark, P.F. Bertone, F. Buchinger, M. Burkey, S. Caldwell, A. Chaudhuri, J.E. Crawford, C.M. Deibel, J. Greene, S. Gulick, D. Lascar, A.F. Levand, G. Li, A. Pérez Galván, K.S. Sharma, J.V. Schelt, R.M. Yee, B.J. Zabransky, Limit on tensor currents from ^{8}Li β decay, Phys. Rev. Lett. 115 (2015) 182501.

[13] N.D. Scielzo, S.J. Freedman, B.K. Fujikawa, P.A. Vetter, Recoil-ion charge-state distribution following the β^{+} decay of ^{21}Na, Phys. Rev. A 68 (2003) 022716.

[14] K. Siegl, N.D. Scielzo, A. Czeszumska, J.A. Clark, G. Savard, A. Aprahamian, S.A. Caldwell, B.S. Alan, M.T. Burkey, C.J. Chiara, J.P. Greene, J. Harker, S.T. Marley, G.E. Morgan, J.M. Munson, E.B. Norman, R. Orford, S.W. Padgett, A. Pérez Galván, K.S. Sharma, S.Y. Strauss, Recoil ions from the β decay of ^{134}Sb confined in a Paul trap, Phys. Rev. C 97 (2018) 035504.

[15] C. Couratin, X. Fabian, B. Fabre, B. Pons, X. Fléchar, E. Liénard, G. Ban, M. Breitenfeldt, P. Delahaye, D. Durand, A. Méry, O. Naviliat-Cuncic, T. Porobic, G. Quéméner, D. Rodríguez, N. Severijns, J.C. Thomas, S.V. Gorp, Electron shakeoff following the β^+ decay of trapped $^{35}Ar^+$ ions, Phys. Rev. A 88 (2013) 041403(R).

[16] E. Liénard, G. Ban, C. Couratin, P. Delahaye, D. Durand, X. Fabian, B. Fabre, X. Fléchard, P. Finlay, F. Mauger, A. Méry, O. Naviliat-Cuncic, B. Pons, T. Porobic, G. Quéméner, N. Severijns, J.C. Thomas, P. Velten, Precision measurements with LPCTrap at GANIL, Hyperfine Interact. 236 (2015) 1–7.

[17] X. Fabian, X. Fléchar, B. Pons, E. Liénard, G. Ban, M. Breitenfeldt, C. Couratin, P. Delahaye, D. Durand, P. Finlay, B. Guillon, Y. Lemiére, F. Mauger, A. Méry, O. Naviliat-Cuncic, T. Porobic, G. Quéméner, N. Severijns, J.C. Thomas, Electron shakeoff following the β^+ decay of $^{19}Ne^+$ and $^{35}Ar^+$ trapped ions, Phys. Rev. A 97 (2018) 023402.

[18] J.A. Behr, A. Gorelov, β-Decay angular correlations with neutral atom traps, J. Phys. G: Nucl. Part. Phys 41 (2014) 114005.

[19] R.M. Yee, N.D. Scielzo, P.F. Bertone, F. Buchinger, S.A. Caldwell, J.A. Clark, C.M. Diebel, J. Fallis, J.P. Greene, S. Gulick, D. Lascar, A.F. Levand, G. Li, E.B. Norman, M. Pedretti, G. Savard, R.E. Segel, K.S. Sharma, M.G. Sternberg, J.V. Schelt, B.J. Zabransky, β-Delayed neutron spectroscopy using trapped radioactive ions, Phys. Rev. Lett. 110 (2013) 092501.

[20] N.D. Scielzo, G. Li, M.G. Sternberg, G. Savard, P.F. Bertone, F. Buchinger, S.A. Caldwell, J.A. Clark, J. Crawford, C.M. Diebel, J. Fallis, J.P. Greene, S. Gulick, A.A. Hecht, D. Lascar, J.K.P. Lee, A.F. Levand, M. Pedretti, R.E. Segel, H. Sharma, K.S. Sharma, I. Tanihata, J.V. Schelt, R.M. Yee, B.J. Zabransky, The β-decay Paul Trap: A radiofrequency-quadrupole ion trap for precision β-decay studies, Nucl. Instrum. Methods Phys. Res. A 681 (2012) 94–100.

[21] A. Czeszumska, N.D. Scielzo, S.A. Caldwell, J.A. Clark, G. Savard, B.S. Wang, A. Aprahamian, M.T. Burkey, C.J. Chiara, J. Harker, A.F. Levand, S.T. Marley, G. Morgan, J.M. Munson, E.B. Norman, A. Nystrom, R. Orford, S.W. Padgett, A. Pérez Galván, K.S. Sharma, K. Siegl, S.Y. Strauss, β-Delayed neutron emission studies of $^{137,138}I$ and $^{144,145}Cs$ performed with trapped ions, Phys. Rev. C 101 (2020) 024312.

[22] B.S. Wang, S.A. Caldwell, N.D. Scielzo, A. Czeszumska, J.A. Clark, G. Savard, A. Aprahamian, M.T. Burkey, C.J. Chiara, J. Harker, A.F. Levand, S.T. Marley, G.E. Morgan, J.M. Munson, E.B. Norman, A. Nystrom, R. Orford, S.W. Padgett, A. Pérez Galván, K.S. Sharma, K. Siegl, S.Y. Strauss, β-Delayed-neutron studies of $^{135,136}Sb$ and ^{140}I performed with trapped ions, Phys. Rev. C 101 (2020) 025806.

[23] J.M. Munson, K. Siegl, N.D. Scielzo, B.S. Alan, A. Czeszumska, G. Savard, A. Aprahamian, S.A. Caldwell, C.J. Chiara, J.A. Clark, J.P. Greene, J. Harker, S.T. Marley, G.E. Morgan, E.B. Norman, R. Orford, S.W. Padgett, A.P. Galvan, K.S. Sharma, S.Y. Strauss, Recoil-ion detection efficiency for complex β decays studied using the Beta-decay Paul Trap, Nucl. Instrum. Methods Phys. Res. A 898 (2018) 60–66.

[24] The AME2020 atomic mass evaluation. II Tables, graphs and references, Chin. Phys. C 45 (3) (2021) 030003.

[25] B.C. Rasco, K.P. Rykaczewski, A. Fijałkowska, M. Karny, M. Wolińska-Cichocka, R.K. Grzywacz, C.J. Gross, D.W. Stracener, E.F. Zganjar, J.C. Blackmon, N.T. Brewer, K.C. Goetz, J.W. Johnson, C.U. Jost, J.H. Hamilton, K. Miernik, M. Madurga, D. Miller, S. Padgett, S.V. Paulauskas, A.V. Ramayya, E.H. Spejewski, Complete β-decay pattern for the high-priority decay-heat isotopes ^{137}I and ^{137}Xe determined using total absorption spectroscopy, Phys. Rev. C 95 (2017) 054328.

[26] H. Ohm, M. Zendel, S. Prussin, W. Rudolph, A. Schröder, K.L. Kratz, C. Ristori, J.A. Pinston, E. Monnand, F. Schussler, J.P. Zirnheld, Beta-delayed neutrons and high-energy Gamma-rays from decay of ^{137}I, Z Physik A 296 (1980) 23–33.

[27] B. Fogelberg, H. Tovedal, Energy levels in ^{137}Xe populated in the decay of the delayed neutron precursor ^{137}I, Nuclear Phys. A 345 (1980) 13–33.

[28] D. Abriola, B. Singh, I. Dillmann, Summary Report of Consultants' Meeting on Beta-Delayed Neutron Emission Evaluation, Tech. rep., International Atomic Energy Agency, 2011.

[29] I. Dillman, P. Dimitriou, B. Singh, Summary report of the 1st research coordination meeting: Development of Reference Database for Beta-Delayed neutron emission, IAEA International Nuclear Data Committee Report, 2013, https://www-nds.iaea.org/publications/indc/indc-nds-0643.pdf.

[30] L. Mathieu, et al., New neutron long-counter for delayed neutron investigations with the LOHENGRIN fission fragment separator, J. Inst. 7 (2012) P08029.

[31] S. Das, The importance of delayed neutrons in nuclear research – a review, Nucl. Energy 28 (1994) 209.

[32] W. Paul, Electromagnetic traps for charged and neutral particles, Rev. Modern Phys. 62 (1990) 531.

[33] D. Manura, Computer code SimIon 3D, version 8.0, Scientific Instrument Services, Inc., 2008.

[34] S. Agostinelli, et al., GEANT4 — a simulation toolkit, Nucl. Intr. Meth. Phys. Res. A 506 (2003) 250.

[35] N.D. Scielzo, S.J. Freedman, B.K. Fujikawa, P.A. Vetter, Measurement of the β-ν correlation using magneto-optically trapped ^{21}Na, Phys. Rev. Lett. 93 (2004) 102501.

[36] B.R. Holstein, Recoil effects in allowed beta decay: The elementary particle approach, Rev. Modern Phys. 46 (1974) 4.

[37] A.H. Snell, F. Pleasonton, Charge spectrometry for Xe^{133}-Cs^{133}, Phys. Rev. 111 (1958) 1338.

[38] A.H. Snell, F. Pleasonton, Ionization following beta decay in Krypton-85, Phys. Rev. 107 (1957) 740.

[39] T.A. Carlson, Electron Shakeoff following the β^- decay of Ar^{41}, Phys. Rev. 131 (1963) 676.

[40] A. Czeszumska, β-Delayed neutron studies of $^{137-138}I$ and $^{144-145}Cs$ performed with trapped ions, (Ph.D. thesis), University of California, Berkeley, 2016.

[41] S.A. Caldwell, A trapped-ion technique for beta-delayed neutron studies, (Ph.D. thesis), University of Chicago, 2015.

[42] K.L. Kratz, W. Rudolph, H. Ohm, H. Franz, M. Zendel, G. Herrmann, S.G. Prussin, F.M. Nuh, A.A. Shihab-Eldin, D.R. Slaughter, W. Halverson, H.V. Klapdor, Investigation of beta strength functions by neutron and gamma-ray spectroscopy (I). The decay of ^{87}Br, ^{137}I, ^{85}As and ^{135}Sb, Nuclear Phys. A 317 (1979) 335–362.

[43] P. Hoff, B. Ekström, B. Fogelberg, The low energy β-strength of ^{135}Sb, Z. Phys. A - Atomic Nuclei 332 (1989) 407–411.

[44] R.L. Craun, D.L. Smith, Analysis of response data for several organic scintillators, Nucl. Instrum. Methods 80 (1970) 239–244.